Case Studies in Thermal Engineering 14 (2019) 100428

Contents lists available at ScienceDirect

Case Studies in Thermal Engineering

journal homepage: www.elsevier.com/locate/csite

Experimental and unsteady CFD analyses of the heating process of large size forgings in a gas-fired furnace

Nima Bohlooli Arkhazloo[a,*], Yassine Bouissa[a], Farzad Bazdidi-Tehrani[b], Mohammad Jadidi[b], Jean-Benoît Morin[c], Mohammad Jahazi[a]

[a] Département de Génie Mécanique, École de Technologie Supériere, Montréal, H3C 1K3, Canada
[b] School of Mechanical Engineering, Iran University of Science and Technology, Tehran, 16846-13114, Iran
[c] Finkl Steel Inc., 100 McCarthy, Saint-Joseph-de-Sorel, QC, J3R 3M8, Canada

ARTICLE INFO

Keywords:
Heat treatment
CFD simulation
Gas-fired furnace
Temperature measurement
Heating uniformity
Radiation modeling

ABSTRACT

Comprehensive unsteady analysis of large size forged blocks heating characteristics in a gas-fired heat treatment furnace was carried out employing experimentally measured temperatures and computational fluid dynamics (CFD) simulations. Heat and fluid flow interactions, consisting of turbulence, radiation and combustion, were simultaneously considered using $k-\varepsilon$, DO and EDM models in a three dimensional CFD model of the furnace, respectively. Applicability of the S2S radiation model was also evaluated to quantify the effect of participating medium and radiation view factor in the radiation heat transfer. Temperature measurements at several locations of an instrumented large size forged block and the furnace chamber were performed. A maximum deviation of about 7% was obtained between the model predictions and the experimental measurements. Results showed that despite the unloaded furnace had uniform temperature distribution, after loading, product surfaces experienced different heating rates, resulting in temperature differences up to 200 K. Findings were correlated with furnace geometry, vortical structures and flow circulations around the workpiece. Besides, S2S model demonstrating reliable results highlighted the importance of radiation view factor optimization in this application. The study could directly be employed for optimization of the heat treatment process of large size steel components.

1. Introduction

A significant number of high strength steel parts used for critical applications in energy and transportation industries acquire their required properties through a sequence of heat treatment processes often called Quench and Temper (Q&T) [1]. The heating process is one of the most important steps since major microstructural changes (grain refinement, phase transformation, etc.) take place, that have a direct impact on the final mechanical properties [2]. Hence, heat transfer from the furnace to the work piece, which fundamentally depends on the temperature distribution inside the furnace, significantly influences the quality of the final product [3]. The process becomes more critical when it comes to the heat treatment of large size parts, such as turbine shafts. Specifically, a non-uniform temperature distribution may result in local changes in the microstructure, leading to non-uniform properties in different

* Corresponding author.
E-mail addresses: nima.bohlooli-arkhazloo.1@ens.etsmtl.ca (N. Bohlooli Arkhazloo), yassine.bouissa@gmail.com (Y. Bouissa), bazdid@iust.ac.ir (F. Bazdidi-Tehrani), jadidi.cfd@gmail.com (M. Jadidi), jbmorin@finkl.com (J.-B. Morin), mohammad.jahazi@etsmtl.ca (M. Jahazi).

https://doi.org/10.1016/j.csite.2019.100428
Received 19 February 2019; Received in revised form 6 March 2019; Accepted 9 March 2019
Available online 14 March 2019

Nomenclature

a	Absorption coefficient
3D	Three dimensional
CFD	Computational Fluid Dynamics
DO	Discrete ordinates model
E	Energy
$_g$	Gravity (m/s^2)
J_i^z	Diffusive flux of chemical species
h	Enthalpy (j/kg)
I	Radiation intensity
k	Turbulence kinetic energy (m^2/s^2)
$\dot{m}$	Mass flux $(kg/m^2.\ s)$
n	Refractive index
p	Pressure (Pa)
$q_i q_r$	The generic source term and reaction heat term respectively
$\vec{r}$	Position vector
R_z	Production rate of z_{th} component
$R_{z,r}$	Production rate of z_{th} component in the reaction
Re	Reynolds number (ud/μ)
Sc	Schmidt number
S_z	Source term of z_{th} component
$s, \vec{s}, \vec{s'}$	Path length, direction vector and scattering direction vector, respectively
$tt_T T$	Time (s), Total heat treatment time (s) and temperature (k), respectively
u_i	Favre-averaged velocity in tensor notation
u_i''	Resolved fluctuating velocity components
Y	Mass fraction of species
x, y, z	Direction of coordinate axes
ε	Turbulence dissipation rate (m^2/s^3)
Ω'	Solid angle
τ_{ij}	Viscous stress tensor
μ_t	Turbulent eddy viscosity$(kg.\ m/s)$
σ, σ_s	Stefan-Boltzmann constant and scattering coefficient
ρ	Density (kg/m^3)
$\rho\overline{u_i' u_j'}$	Reynolds stress $(kg/m.\ s^2)$
$\langle\rangle$	Favre averaging operator

Superscripts and Subscripts

‘	Fluctuations with respect to a Reynolds averaging
“	Fluctuations with respect to a Favre averaging
i, j, k	Tensorial indices
z	z_{th}species

locations of the final part. Therefore, accurate temperature prediction of the parts necessitates a quantitative analysis of the transient heating and an understanding of thermal interactions within the furnace.

Comprehending the complexities of the thermal field, along with the turbulent fluid flow inside the heat treatment furnace is very challenging. Complicated load-gas-furnace thermal interactions, including transient convection-radiation heat transfer, impose strong non-linear thermal boundary conditions to the load. Chapman et al. [4] employed analytical and Gao et al. [3] used semi analytical methods, to develop general correlations for the heat treatment schedule and temperature evolution of products. However, analytical studies are generally limited to linear problems and become very complex when non-linear transient conditions or interactions between phenomena are included. On the other hand, experimental measurements in this particular field of study are very challenging; especially, in the case of large size products, reliable data acquisition during the process is more complex.

Therefore, numerical methods such as computational fluid dynamics (CFD) offering simultaneous analysis of turbulent fluid flow, combustion and conjugate heat transfer could be an excellent tool for simulating and subsequently optimizing the heat treatment process. 3D full scale numerical models are critical in the implementation process of smart manufacturing technology' (industry 4.0) practices. Different furnaces such as electrically heated or gas quenching furnaces have been studied using CFD [5–7]. However, among the above furnaces, the simulation of the heat treatment in gas-fired furnaces are more complex due to reactive flow combined with turbulent transport and conjugate heat transfer including absorbing and emitting hot combustion products. Inherently, the problem is more acute when it comes to large size furnaces and therefore little data is available in the scientific literature. Recently, Liu et al. [8] using CFD, proposed a basic model for increasing the uniformity in continues gas-fired furnaces. Mayr et al. [9] used a one-step steady state CFD approach and Tang et al. [10] a combination of 3D CFD and 2D finite difference methods to predict temperature evolution in pusher type gas fired furnaces. However, very little data is available on large size batch type furnaces. Besides, most of the experimental studies have been used as a validation tool of the simulation. The limited published studies have been devoted to one aspect of the process (i.e., burner positions, furnace chamber, or product heating characteristics). For example, Danon et al. [11] assessed burner positioning effects on the performance of multi-burner combustion furnace and Galletti et al. [12] mainly focused on different combustion models for the burner simulation inside a semi-industrial furnace. Prieler et al. [13] employing experimental validation demonstrated the applicability of CFD for combustion modeling of flat burners in a lab-scale heat treatment furnace. Recently, Mayr et al. [14] presented a combustion model, with lower computational demand, for semi-industrial gas-fired furnaces.

The objective of the present study is therefore to carry out a comprehensive analysis of heat transfer in the heat treatment process of forged blocks in a large size gas-fired furnace employing both experimental measurements and CFD simulation. The experimental data was generated through the instrumentation of the furnace chamber (loaded and unloaded) as well as the different surfaces of the block during the heat treatment process. Unsteady CFD analysis using a combination of $k-\varepsilon$, EDM and DO models was employed to identify the effects of different geometrical and process related parameters on corresponding heat transfer modes. In addition, S2S radiation model was employed to assess its applicability in this type of heat treatment furnaces and to quantify the effect of radiation heat transfer parameters on the temperature evolution of the product.

2. Experimental procedures

The instrumented furnace was a 3.05 × 3.28 × 11.63 (m^3) car bottom gas-fired furnace equipped with 18 high-velocity cup burners [15] located on the two sides of the furnace, along the Z direction with 9 burners on the upper section of the furnace left wall, (upper burners) and the 9 other in the lower section of the right wall (lower burners). Under ideal operational conditions, the burner flame length and the combustion product velocity at the exit of burner should be 0.508 (m) and 107 (m/s), respectively. Nine fixing bars with a cross section of 0.25 (m) × 0.25 (m) and a length of 2.60 (m) are positioned between the burners for placing the forged ingots. The furnace was operated under a positive pressure of approximately 0.2 (mbar) to minimize any air entry. The furnace medium drawings, including the dimensions are provided in Fig. 1(a).

Experimental measurements were divided into two steps of loaded and unloaded furnace to evaluate the loading effect on the temperature distribution inside the furnace and on the forged block. Sixteen-standard sheathed k-type thermocouples (TC) were installed at different positions of the unloaded furnace; and temperature evolution during an entire heat treatment cycle (i.e. heating, isothermal holding, and cooling). The results were used both to confirm the temperature uniformity of the furnace and to provide a basis for the heat transfer analysis of the loaded furnace.

Also, Temperature evolution in the loaded furnace was recorded by placing 11 k-type TCs at different locations of a 1.4 × 0.89 × 2.72 (m^3) forged block. These thermocouples were fixed to the different surfaces of the block to evaluate the heating pattern around the workpiece (See Fig. 1(b)). To ensure a solid attachment of all TCs, small holes were drilled and TCs were solidly embedded at the bottom of the holes. The empty space of the hole was filled with iron powder of the same steel and the top of the hole was sealed with iron cement and a fixing screw. The standard accuracy of the K-type thermocouples with a stainless steel sheath is equal to Ref. $\pm 0.75 \times T$[16], which corresponds to an accuracy of ± 6.63 (K) for the furnace operating temperature ranges. Considering the large size of the furnace and workpiece, extensive care was taken to insure accurate installation of the 11 TCs and exact positioning and alignment of forged ingot on the car-bottom furnace; however, a 1–2 cm error was estimated in the determination of probes positioning. In order to simulate heat transfer conditions, as close as possible to real operational conditions, two other forged blocks with 1.4 × 0.79 × 2.72 (m^3) dimensions were also placed in the front and back of the instrumented block.

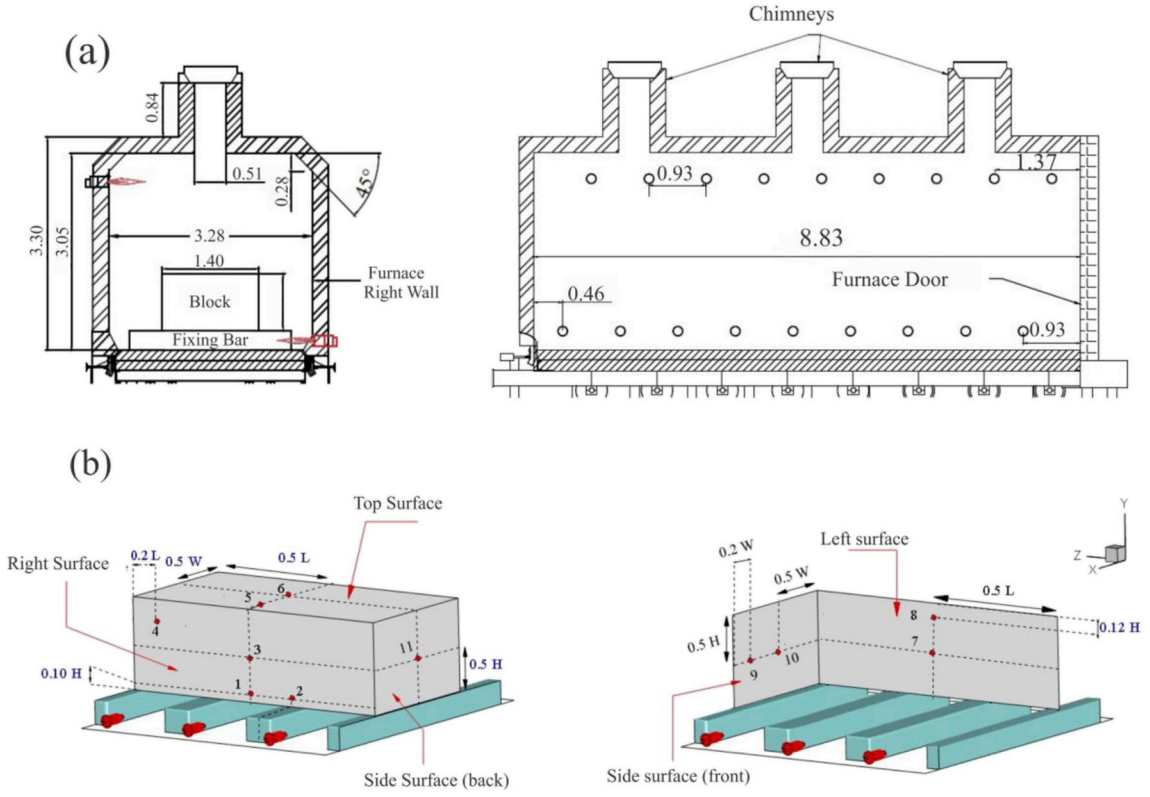

Fig. 1. (a) Dimensions and geometry of the car bottom gas-fired furnace and (b) Schematic views of thermocouples locations on the instrumented forged ingot.

3. Computational details

3.1. Flow simulation

A transient CFD simulation applying a pressure-based solver was employed to solve the density weighted Reynolds-averaged Navier-Stokes (RANS) equations, as follows [17].

$$\frac{\partial \tilde{\rho} u_i}{\partial x_i} = 0 \tag{1}$$

$$\frac{\partial \tilde{\rho} u_i u_j}{\partial x_i} = \frac{\partial \tilde{\rho} u_i'' u_j''}{\partial x_i} - \frac{\partial p}{\partial x_i} + \frac{\partial \tau_{ij}}{\partial x_i} + \tilde{\rho} g_i \tag{2}$$

$$\frac{\partial \tilde{\rho} h u_i}{\partial x_i} = \frac{\partial \tilde{\rho} h'' u_i''}{\partial x_i} + \frac{\partial \tilde{p}}{\partial t} - \frac{\partial \tilde{J}_i^z}{\partial x_i} + \tau_{ij} \frac{\partial u_i}{\partial x_i} + q_i + q_r \tag{3}$$

$$\frac{\partial \tilde{\rho} Y_z u_i}{\partial x_i} = -\frac{\partial \tilde{\rho} Y_z'' u_i''}{\partial x_i} - \frac{\partial \tilde{J}_i^z}{\partial x_i} + \dot{R}_z \tag{4}$$

where, the stress tensor, τ_{ij}, is given by:

$$\tau_{ij} = \left[\mu \left(\frac{\partial u_i}{\partial x_j} + \frac{\partial u_j}{\partial x_i} \right) \right] - \frac{2}{3} \mu \frac{\partial u_i}{\partial x_j} \delta_{ij} \tag{5}$$

and the diffusive flux of combustion product species is defined by the Fick's law:

$$\tilde{J}_i^z = \frac{\mu_t}{Sc_k} \frac{\partial Y_z}{\partial x_i} \tag{6}$$

The definition of all the variables and related units are provided in the nomenclature page. According to the literature [18], the two-equation standard $k-\varepsilon$turbulence model [19], could be reliably used to determine the turbulence associated with the gas combustion in the gas-fired furnaces by solving the additional turbulence kinetic energy (k) and dissipation rate (ε) equations [19].

3.2. Radiation modeling

In the present work, the discrete ordinates (DO) model [20] was used to solve the radiative transfer equation (RTE), Eq. (7), considering the absorption and emission effects.

$$\frac{dI(\vec{r}, \vec{s})}{ds} + (a + \sigma_s) I(\vec{r}, \vec{s}) = an^2 \frac{\sigma T^4}{\pi} + \frac{\sigma_s}{4\pi} \int_0^{4\pi} (\vec{r}, \vec{s})(\vec{r}, \vec{s}) \phi(\vec{r}, \vec{s}) d\Omega' \tag{7}$$

I is the radiation intensity and $(a + \sigma_s)s$is the optical thickness of the medium. Due to the presence of combustion products the weighted-sum-of-gray-gases model (WSGGM) using the coefficients provided by Smith et al. [21] was employed to compute the radiative properties inside the furnace. For WSGGM model, the domain-based approach was employed to calculate the mean beam length [17].

The applicability of the S2S model, as a computationally effective method in the optically thin medium, was also evaluated in the present work along with the DO model. The S2S model assumes any absorption, emission, or scattering of radiation by the medium can be ignored; thereby, reducing the computational cost by only considering the surface-to-surface radiation. In this model, the radiation heat transfer to a surface from another surface is a direct function of the surface-to-surface view factor. Therefore, the radiation energy balance for each surface follows Eq. (8).

$$q_{out,k} = \varepsilon_k \sigma T_k^4 + \rho_k \sum_{j=1}^{N} F_{kj} q_{out,j} \tag{8}$$

$F_{kj}$is the view factor between surface k and surface j.

3.3. Combustion modeling

Combustion inside the burner and furnace domains was modeled using the eddy-dissipation model (EDM). It should be noted that, because in the gas-fired furnace the burners create high velocity combustion products, the Arrhenius chemical kinetic calculations were not considered thereby the computational cost is significantly reduced. In EDM, the species transport formulation for the local mass fraction species (Y_z), for the z_{th} species, was solved assuming that the reaction rates were dominated by turbulence [22]. Therefore, the species transport equation becomes as follows [17]:

$$\frac{\partial}{\partial t}(\rho Y_z) + \nabla.(\rho \bar{v} Y_z) = -\nabla.\overline{J_z} + \dot{R}_z + \dot{S}_z \tag{9}$$

In the above equation, the reaction rate is calculated on the basis of eddy mixing scale, k/ε, and the eddy-break [19].

3.4. Numerical simulation procedure and boundary conditions

CFD simulations were carried out using the finite-volume based ANSYS-FLUENT software [17]. The unsteady SIMPLE algorithm [23] was applied to 15,155,000 hexahedral non-uniform computational grids as illustrated in Fig. 2. Grid value includes 356,000 non-uniform cells in each burner domain (6,408,000 in total for 18 burners) and finer grids near the burner exit to capture the combustion phenomenon and heat and fluid flow coming from burners to the furnace domain. Non-uniformly distributed grids with finer grid sizes near the walls and burner interfaces were employed to consider the effects imposed by velocity and thermal boundary layers. Averaged heat loss of 594 (W/m2), calculated based on the approach proposed by Hadata et al. [24], was applied to the furnace walls. The emissivity of the furnace refractories and the steel workpiece were set to 0.75 and 0.8 (corresponding to an oxidized steel surface), respectively (See Table 1). The mass flow inlet boundary conditions with averaged values of 0.018 (kg/s) and 0.516 (kg/s) were considered for the gas and air inlets, respectively, while pressure outlet was considered for the chimney exhaust. Calculations at each time step continued up to a convergence criterion of 10^{-5}, 10^{-6} and 10^{-9} for the continuity, energy and radiation equations, respectively.

4. Results and discussion

4.1. Experimental analysis

The uniformity test results of the unloaded furnace showed a very conformity with the predefined heating pattern with maximum standard deviation values of 5.28 (°C) during the ramp stage with the furnace increasing its temperature to reach the target temperature. Therefore, it can be considered that the unloaded furnace presents a good temperature uniformity over its entire volume during the entire heat treatment cycle.

The measured temperature histories of different locations of the forged block are illustrated in Fig. 3. The results reveal a clear difference in temperature evolution as a function of the location of the TCs (i.e. considered face and TCs position on the surface).

Usually, severity and continuity of the temperature gradient between the surface and the center of the workpiece is one of the main concerns of steel making industries, as it directly impacts the quality of the final product [1]. However, Fig. 3(a) shows that apart from the temperature gradient inside the workpiece, differences in temperature can also be found on the surfaces themselves (see Fig. 1 for locations of TCs). Although, temperatures of all TCs on the surfaces ultimately converge to the target pre-defined temperature at the end of the process, the temperature histories of different points of the forged ingot are not identical. This variability in the heating history could affect the microstructural transformations from one end to another end of the product (subsequently its properties), and needs to be taken into consideration when developing microstructure based models of phase transformation.

As indicated in Fig. 3, it is clear that the TC on the right surface (TC.1), located at a shorter distance to the burner (lower burners), had higher temperatures in comparison to those of the left and the top surfaces. Besides, TCs of the side surfaces (TC.10 and TC.11) had the minimum temperatures during the process. These surfaces, due to their relative positions in the furnace, were faced with adjacent forged blocks instead of furnace walls or burners; i.e., they had limitations regarding any direct thermal radiation from the furnace and due to the small gap between the blocks, they had relatively smaller radiation view factors from the furnace parts.

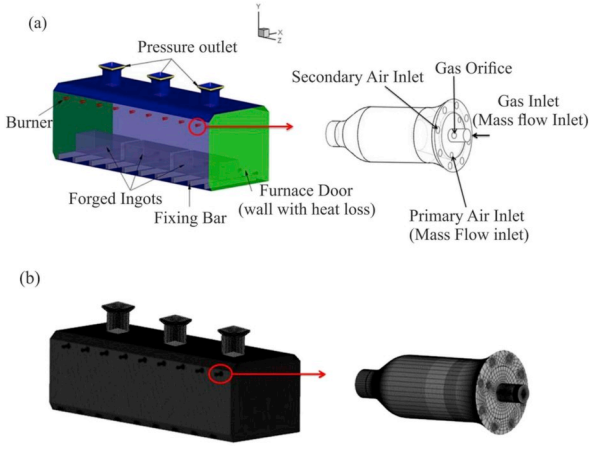

Fig. 2. Computational domain, including: (a) boundary conditions and (b) computational grids.

Table 1
Chemical analysis of the test forged ingot used for thermo-physical properties calculation- % weight [25].

C	Mn	Si	Mo	Cr	Ni	Other
0.35	0.85	0.4	0.45	1.85	0.47	Micro alloying

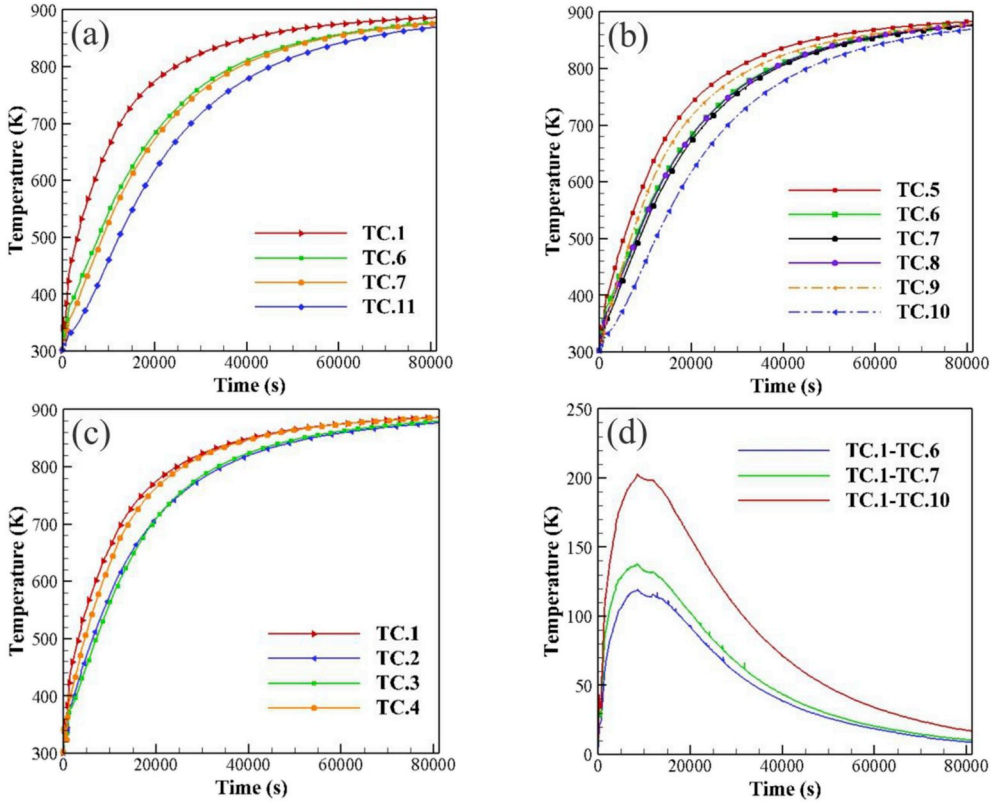

Fig. 3. Experimentally measured temperature evolution of TCs on: (a) different surfaces of the forged ingot, (b) left, top and side surfaces, (c) right surface and (d) their relative temperature differences.

Fig. 3(b) also shows that among the thermocouples on the other surfaces, those that are closer to the right surface or product edges (TC.5, TC.8 and TC.9) had higher values. The edge effect is also visible in Fig. 3(c) where it can be seen that TC.4 has relatively higher temperatures as compared with the TC.3 and TC.2 on the same surface. Another interesting finding is the relatively lower temperatures of the TC.2, which was located above the fixing bar on the right surface. Although TC.2 had a relatively short distance to the burner, in comparison with TC.4 and TC.3, it experienced lower temperatures.

Finally, the temperature differences between selected thermocouples in different faces are presented in Fig. 3(d). It can be seen that the maximum difference between TC.1 (on the right surface) and TC.10 (on the side surface) could reach up to 200 K. Further, this difference for TC.1-TC.6 and TC.1-TC.7 could reach up to 140 K and 120 K, respectively. Considering the previously discussed initial temperature uniformity of the unloaded furnace at different temperatures, the observed non-uniformity could be correlated to the presence of the forged ingots. Therefore, the transient heating history should be analyzed by considering both convection and radiation heat transfer modes.

4.2. CFD analysis

To comprehensively analyze the heating patterns, temperature non-uniformities and the share of each heat transfer mode during

Table 2
Predicted heat distribution within the furnace.

Item	Ingots	Walls	Flue Gas	Fixing Bars	Other
Absorbed/lost heat (GJ)	28.08	7.65	25.74	9.2	5.42

the heat treatment process, CFD simulations results are discussed in this section.

4.2.1. Validation

Table 2 shows the distribution of the available heat in different parts of the furnace, obtained from the CFD analysis. The furnace efficiency was defined by the ratio of the net heat received by the forged blocks and the available heat input to the furnace (78 GJ) as follows [9]:

$$\eta_{furnace} = \frac{Q_{ingot}}{Q_{available}} \tag{10}$$

Based on the measurements made on the gas flow meters installed on the furnace, furnace efficiency was estimated to be 36.6%, while the CFD simulation predicted a value of 40.1%, which are quite close considering the large size of the furnace. The observed difference is probably due to a combination of factors such as air leakage into the furnace and difference in the exact location of the TCs between the experimental and modeled conditions, that can not be really predicted by the model.

Results of the numerically predicted and experimentally measured temperatures at different locations of the block are presented in Fig. 4(a). The CFD model predicts the temperature evolution fairly well with a maximum deviation of about 7%, which is mostly related to the initial heating stage. As mentioned above, the differences between the experimental and simulation results are reasonable considering the large dimensions of the furnace and the blocks. Although some over-predictions can be observed for the surface temperatures, Fig. 4(a) shows that the simulation results are valid and further investigation can be carried out using the present CFD model. Therefore, models such as standard $k-\varepsilon$with a relatively lower computational cost in comparison with the more complex ones (such as the RSM turbulence model) can be employed effectively in this application for furthered detailed studies or optimization purposes. Nonetheless, employment of more sophisticated models such as RSM and their related boundary conditions for turbulence modeling or increasing the mesh size could result in better accuracy. Also, increasing the number of control angles in the angular discretization of the DO model could result in more accurate predictions of the local thermal radiation, where strong variations of spatial temperatures exist (i.e., the burner area). However, these recommendations will add to the computational costs in the solution procedure and therefore, computational cost/benefit analysis needs to be carried out on a case by case basis.

Radiation view factor of the workpiece surfaces and participating medium are the two main active parameters for the analysis of the radiation heat transfer, in the present application. The influence of participating medium on the final temperature history was evaluated using the S2S model and the results are reported in Fig. 4(b). It can be seen that, neglecting the effect of combustion products participation in the absorbed radiation of the workpiece, characteristic of the S2S model, produces about 1.5% over prediction in comparison to the DO model. Thus, although DO model provides more accurate predictions, S2S model with lower computational cost, can be effectively used in this application. Furthermore, because 98.5% of radiation heat transfer is controlled by the radiation view factor of the surfaces, loading pattern optimization for this type of furnaces can be done only by view factor optimization when the radiative heat transfer is considered.

4.2.2. Analysis of the heating process of the loaded furnace

Transient contours of temperature evolution of the loaded furnace (in an x-y plane) and ingot surfaces during the heating process are depicted in Fig. 5. The simulation results clearly confirm a non-uniform temperature distribution during the heating process as observed during the experimental phase (Fig. 3). Ingot transient temperature history shows that the side surfaces have relatively lower temperatures in comparison with the other surfaces. Gradual heating from the right surface to the left and top surfaces and finally side surfaces is evident. A maximum temperature difference of about 262 K exists from one side of the product to the other.

Results of furnace heating history show that the temperature of the furnace starts increasing from regions close to the burners and then gradually extends to the center. Similarly, an increase in temperature begins rapidly on the right side of the block where the lower burners are located; while the left and side surfaces are heated latterly. Results also indicate that the fluid in the vicinity of the

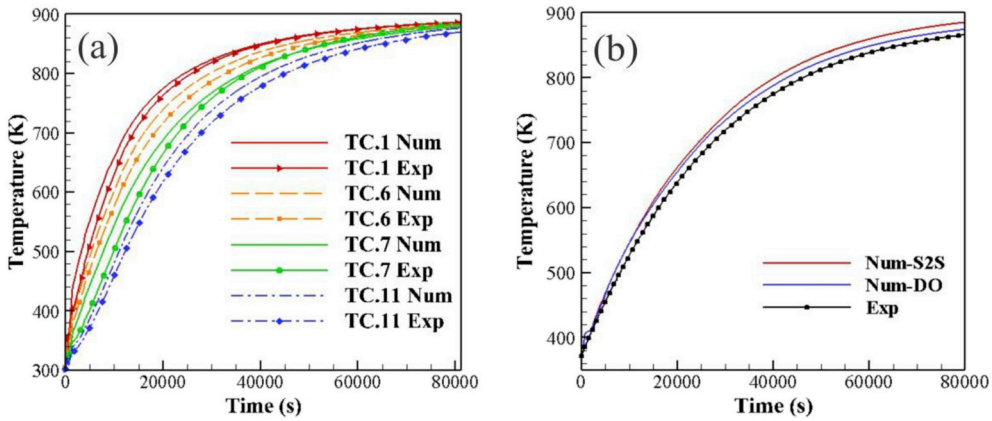

Fig. 4. Comparison between numerically predicted and measured temperatures of the workpiece.

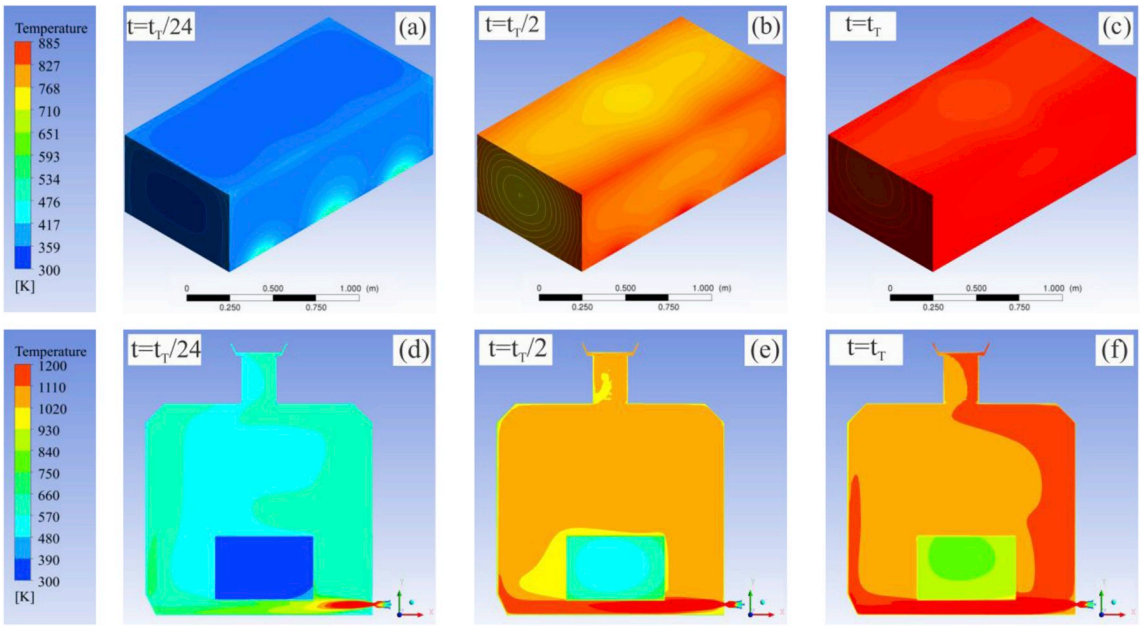

Fig. 5. Transient contours of temperature evolution of the furnace and forged ingot surfaces.

left surface and the top surface was also heated with delay in comparison with the right surface where the lower part of the right surface hindered the fluid flow circulation (Fig. 5(e)). These findings further confirm the results reported in experimental measurements.

Fig. 6 shows the transient history of average total heat flux, average radiation heat flux and average surface heat transfer coefficient on the right, left and side surfaces of the workpiece during the heat treatment process. A considerable difference between

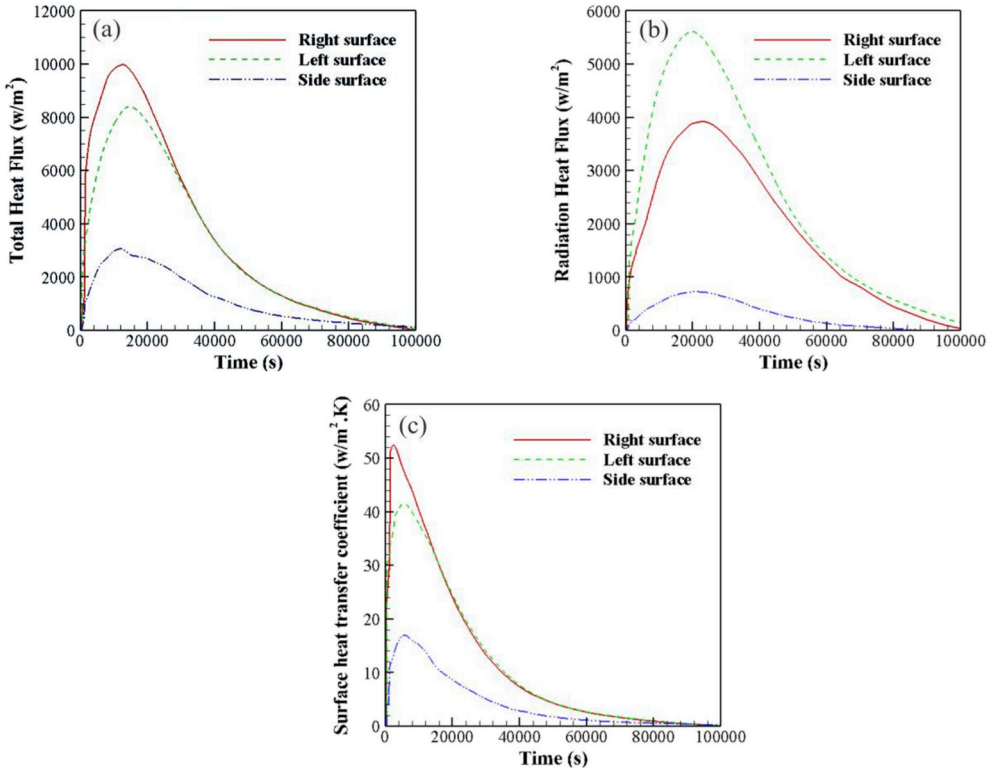

Fig. 6. Transient history of a) total heat flux b) radiation heat flux and c) heat transfer coefficient for different surfaces.

the total heat flux rates in the first period of the process is revealed, which is in direct relation to the identified non-uniformities (see Figs. 3 and 4). Both radiation and convection heat transfers modes show the same identified differences in their transient histories. However, as it can be seen, the right surface due to the high velocity of burner product, is mainly heated by the convection heat transfer at the beginning of the process, while for the left surface, radiation heat transfer plays the most important role due to the blockage of the fluid flow by the workpiece. The results indicate that heat transfer coefficient in the first part of the process for the side surface is less than those on the right and left surfaces and in the peak zone its value is 0.32 of the one for the right surface. On the other hand, the radiation heat flux at this surface in the first period of the process was about 12 and 17% of the left and the right surfaces fluxes, respectively. Due to the small gap between the blocks, side surfaces have lower radiation view factors and convection heat transfer coefficients. Therefore, the loading effect by reducing both heat transfer modes (mainly, the radiation heat flux) affects the temperature history of the side surface, whilst for the right and left ones it mainly changes the heat transfer modes and heating pattern.

Local temperature distributions (contours) on the right surface and the bottom surface of the forged ingot are presented in Fig. 7. Three significant temperature gradients (red regions), equal to the number of burners facing the block, are observed. The high temperature region in the middle of the right surface (Fig. 7(a)) has higher temperatures in comparison to the side ones. This could be due to the fact that the side surfaces are affected by gaps between the blocks. High temperatures are also visible near the edges of this surface as shown in Fig. 7(a). Usually, the temperature on the edges is higher relative to the other points due to more radiative heat flux in these regions (more surfaces to absorb radiation from furnace walls and combustion products [9]). However, the results indicate that the edge effect on the temperature distribution of the right surface is not as strong as the burner effect. The temperature gradient on the right surface could reach up to 159 K which shows the importance of burner locations inside the heat treatment furnaces.

The effect of the fixing bars on temperature distribution of the product is illustrated in Fig. 7(b). Two blue colored areas near to the fixing bars at the right surface confirm the measured temperature of the TC.2 in Fig. 3. In addition, Fixing bars covering part of the bottom surface prevent the active radiation and convection heat transfer of the furnace (i.e. these areas are heated by conduction only). The shadow effect of the fixing bars can also have a major effect on temperature distribution inside the forged block. A combination of burner's effect (higher temperatures) and fixing bars shadows (lower temperatures) on the bottom surface is probably the origin of the significant thermal gradient on this surface (up to 251 K). Therefore, the geometrical effect of the furnace such as burner's location and the position of the fixing bars should be carefully taken into account for an accurate and reliable analysis of the heat treatment within large size furnaces.

4.2.3. Analysis of fluid flow structures

The local convection heat transfer to the forged ingot in the context of objects facing with flow stream, called as bluff body, should also be analyzed based on the formation of flow structures (also called as vortical structures or vortices) around the object [26]. It should be noted that the formation of vortical structures around can cause non-uniform temperature distributions on the forged block surfaces [26]. Vortical structures are characterized by different parameters such as size, scale, shape, velocity, vorticity and energy. It has been reported that one of the main characteristics of the vortical structures is the formation of coherent circulation in parts of the flow field [27]. Therefore, fluid flow circulation inside the furnace is visualized in Fig. 8, using time-averaged streamlines at x-y planes. Streamlines show a blockage of fluid flow by the load in the impingement zone (creation of stagnation point) and the formation of a wake region in the downstream (existence of a wake vortex in the vicinity of the left surface). This behaviour can be seen in the formation of vortical structure around a typical bluff body [26]. Fig. 8 shows that there is a clockwise circulation of fluid flow inside the furnace at each section, which is in correlation with the heating trend in the furnace. Fig. 8 also, shows the presence of a strong vortex at the center of the furnace in both planes (perpendicular to the lower burner and between fixing bars). Further, a detachment of fluid from the block near the left side of the top surface and the upper side of the left surface is clear. The coexistence of wake vortices and detachment of fluid near the left surface of the forged ingot and the presence of a cold area in this zone, shows the interrelation between the convection heating pattern and the fluid flow structures inside the furnace. A similar behaviour can also be observed on the top surface and its adjacent vortex. Moreover, creation of a small vortex near the right surface where the burner products faced directly with the forged ingot surface (stagnation point) also indicates the interrelation between forged ingot heating

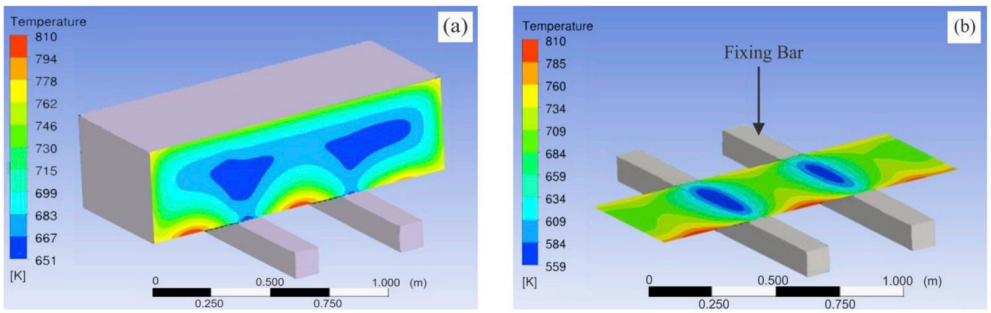

Fig. 7. Contours of temperature distribution on a) right surface and b) bottom surface of the forged ingot at $t = t_T./6$

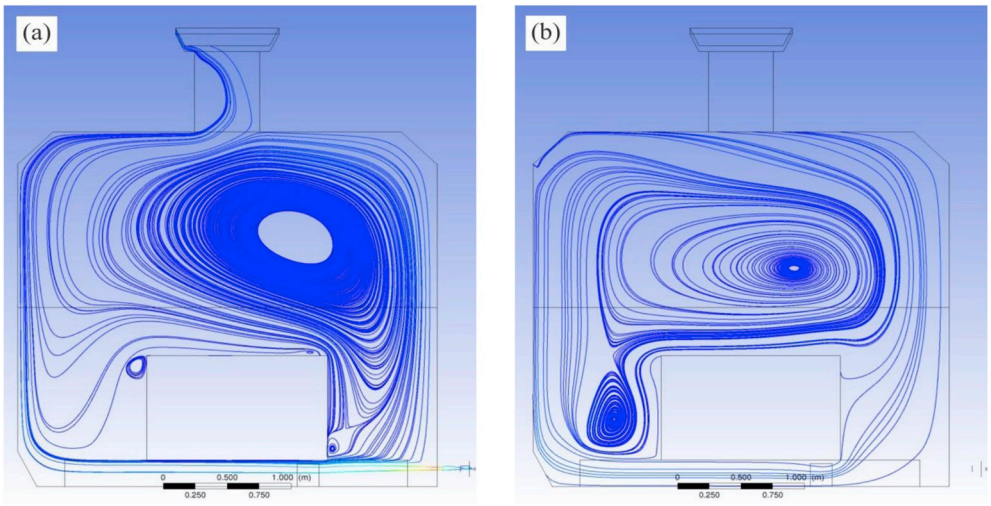

Fig. 8. Streamlines of planes at a) between fixing bars and perpendicular to down burner face and b) center of fixing bars.

and the vortical structures. Therefore, tracking the vortical structures within the furnace should be considered as an important parameter for the process optimization and multiple loading scenarios. The effect of these structures is expected to be more significant at lower temperatures, where the convective heat transfer mode could dominate the radiation one and the maximum non-uniformity identified.

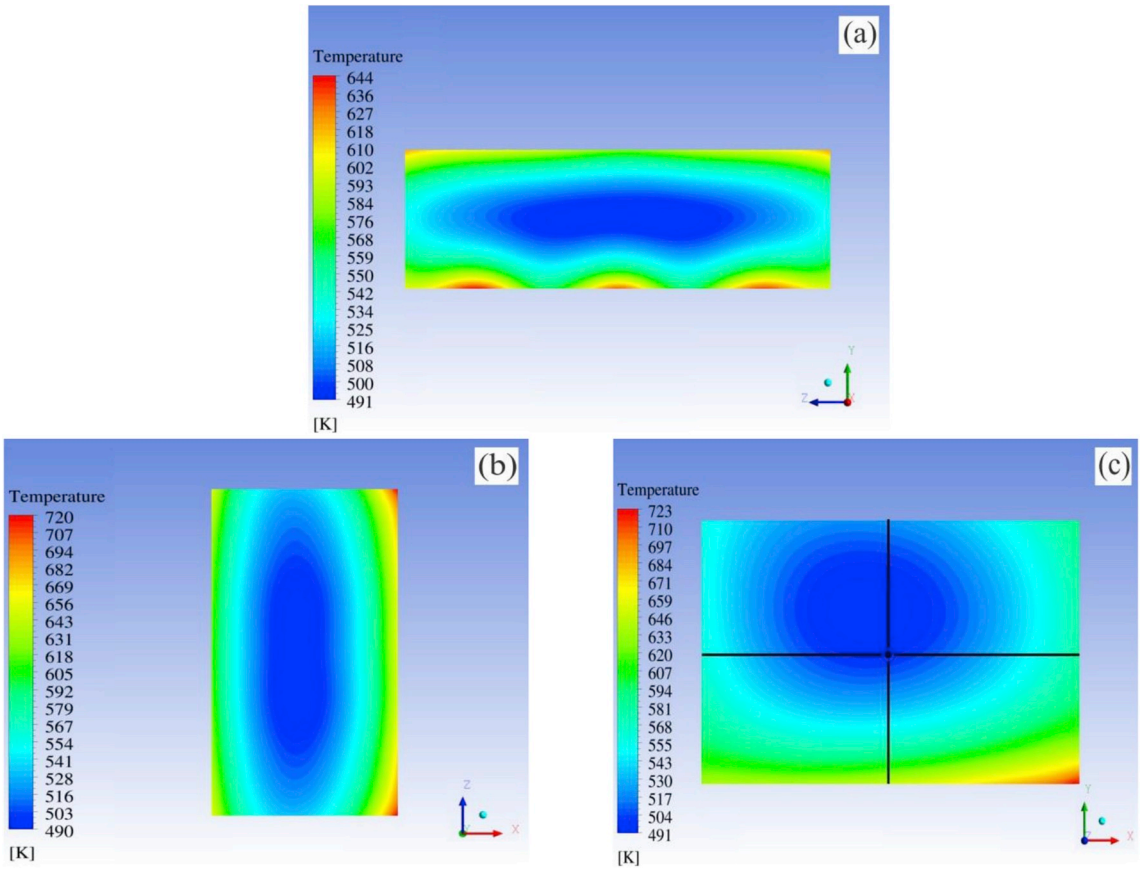

Fig. 9. Temperature contours of cross-sectional planes at the center of the forged ingot in: (a) longitudinal, (b) transversal and (c) lateral planes at $t = t_T/6$

4.2.4. Assessment of heating process inside the large size forgings

Investigation of the temperature distribution inside the block can help to quantify the impact of the non-uniform heating of the surfaces on the temperature evolution inside the forging. It can be seen in Fig. 9 that the central planes also affected by non-uniform heating of the surface and the same pattern of heating from the bottom and right side of the forged block to the left, top and finally side surfaces is visible inside the workpiece. Cold area is mainly extended longitudinally between two side surfaces. Fig. 9(c) also shows that the coldest point in the lateral plane is actually not located at the center of the forged block and shifted toward the left and top surfaces. The results clearly demonstrate that product loading, geometrical parameters and fluid flow circulation around the forged block influence the heating pattern inside the product. However, the strength of the above-mentioned parameters is more visible on the surface temperature distribution, as compared with the inside of the workpiece. Generally, it is assumed that the differentiation in the mechanical properties of the forged ingot mainly varies as a function of the distance from the surface. However, considering the temperature gradient from one side to the other and different temperatures at the same depth of the forged block, the above assessment should be relativized and a more precise approach should consider the heating pattern and its directions.

5. Conclusions

Comprehensive analysis of heat transfer in the heat treatment process of forged blocks in a large size gas-fired heat treatment furnace was investigated in the present work. Experimental temperature measurement and unsteady CFD simulations were employed for simultaneous analysis of fluid flow interactions inside the furnace including turbulent combustion, fluid flow structures and also conjugate heat transfer during the heating. Concluding remarks are summarized as follows:

1. The developed 3D CFD model provided good agreement with experimentally measured data.
2. Both DO and S2S radiation models could be reliably used for this application. An over-prediction of less than 2% was predicted when using the S2S model in comparison with the DO model, which indicates that the computationally effective S2S model can be employed for this type of gas-fired heat treatment furnaces. The analysis of the results also showed that radiation view factor has a higher contribution than participating medium when analyzing radiation heat transfer during heat treatment of large size components.
3. Analysis of experimental temperature measurements showed that the unloaded furnace domain was uniform during the test. However, after loading, temperature non-uniformities, up to 200 K, were found during the heating process, which could affect microstructure evolution.
4. The influence of geometrical effects such as burner locations and fixing bars as sources for temperature non-uniformities must be taken into consideration for optimizing the heat treatment process of large size components.
5. The formation of vortical structures in the turbulent flow field results in significant changes in the convection heat transfer of the affected area, which demonstrates the interrelation between the heating pattern and the fluid flow structures inside the furnace.
6. The developed CFD model was validated using experimental measurements. The obtained data could be directly applied for the optimization of the operational conditions and loading patterns of large size gas-fired heat treatment furnaces.

Funding

This work was supported by the Mitacs in the framework of [IT03151] Grant.

Acknowledgement

The authors are very grateful to Finkl Steel, especially the R & D, Metallurgy and Engineering Departments, for providing the large size bloc, as well as the instrumentation and measurements used in the present research.

References

[1] G.E. Totten, Steel Heat Treatment: Metallurgy and Technologies, CRC Press, 2006.
[2] J. Kang, Y. Rong, Modeling and simulation of load heating in heat treatment furnaces, J. Mater. Process. Technol. 174 (2006) 109–114.
[3] M. Gao, C.N. Reid, M. Jahedi, Y. Li, Estimating equilibration times and heating/cooling rates in heat treatment of workpieces with arbitrary geometry, J. Mater. Eng. Perform. 9 (2000) 62–71.
[4] K.S. Chapman, S. Ramadhyani, R. Viskanta, Modeling and parametric studies of heat transfer in a direct-fired batch reheating furnace, J. Heat Treat. 8 (1990) 137–146.
[5] J. Wang, J. Gu, X. Shan, X. Hao, N. Chen, W. Zhang, Numerical simulation of high pressure gas quenching of H13 steel, J. Mater. Process. Technol. 202 (2008) 188–194.
[6] F. Cosentino, N. Warnken, J.-C. Gebelin, R.C. Reed, Numerical and experimental study of post-heat treatment gas quenching and its impact on microstructure and creep in CMSX-10 superalloy, J. Mater. Process. Technol. 213 (2013) 2350–2360.
[7] X. Hao, J. Gu, N. Chen, W. Zhang, X. Zuo, 3-D Numerical analysis on heating process of loads within vacuum heat treatment furnace, Appl. Therm. Eng. 28 (2008) 1925–1931.
[8] Y.J. Liu, J.D. Li, R.D.K. Misra, Z.D. Wang, G.D. Wang, A numerical analysis of slab heating characteristics in a rolling type reheating furnace with pulse combustion, Appl. Therm. Eng. 107 (2016) 1304–1312.
[9] B. Mayr, R. Prieler, M. Demuth, L. Moderer, C. Hochenauer, CFD analysis of a pusher type reheating furnace and the billet heating characteristic, Appl. Therm. Eng. 115 (2017) 986–994, https://doi.org/10.1016/j.applthermaleng.2017.01.028.
[10] G. Tang, B. Wu, D. Bai, Y. Wang, R. Bodnar, C. Zhou, CFD modeling and validation of a dynamic slab heating process in an industrial walking beam reheating furnace, Appl. Therm. Eng. 132 (2018) 779–789.

[11] B. Danon, E.S. Cho, W. De Jong, D.J.E.M. Roekaerts, Numerical investigation of burner positioning effects in a multi-burner flameless combustion furnace, Appl. Therm. Eng. 31 (2011) 3885–3896, https://doi.org/10.1016/j.applthermaleng.2011.07.036.
[12] C. Galletti, G. Coraggio, L. Tognotti, Numerical investigation of oxy-natural-gas combustion in a semi-industrial furnace: validation of CFD sub-models, Fuel 109 (2013) 445–460.
[13] R. Prieler, B. Mayr, M. Demuth, D. Spoljaric, C. Hochenauer, Application of the steady flamelet model on a lab-scale and an industrial furnace for different oxygen concentrations, Energy 91 (2015) 451–464.
[14] B. Mayr, R. Prieler, M. Demuth, M. Potesser, C. Hochenauer, Computational analysis of a semi-industrial furnace fired by a flat flame burner under different O2/N2ratios using the steady laminar flamelet approach, J. Energy Inst. 90 (2017) 602–612, https://doi.org/10.1016/j.joei.2016.05.002.
[15] C.E. Baukal Jr., Industrial Burners Handbook, CRC press, 2003.
[16] I.S.A. Standard, Temperature Measurement Thermocouples, (1982).
[17] A. Fluent, Fluent 12. Theory Guide, (2017).
[18] Y. Liu, Y. Liu, S. Tao, X. Liu, Z. Wen, Three-dimensional analysis of gas flow and heat transfer in a regenerator with alumina balls, Appl. Therm. Eng. 69 (2014) 113–122.
[19] D.B. Spalding, Mixing and chemical reaction in steady confined turbulent flames, Symp. Combust. Elsevier, 1971, pp. 649–657.
[20] E.H. Chui, G.D. Raithby, Computation of radiant heat transfer on a nonorthogonal mesh using the finite-volume method, Numer. Heat Tran. 23 (1993) 269–288.
[21] T.F. Smith, Z.F. Shen, J.N. Friedman, Evaluation of coefficients for the weighted sum of gray gases model, J. Heat Transf. 104 (1982) 602–608.
[22] B.F. Magnussen, B.H. Hjertager, On mathematical modeling of turbulent combustion with special emphasis on soot formation and combustion, Symp. Combust. Elsevier, 1977, pp. 719–729.
[23] H.K. Versteeg, W. Malalasekera, An Introduction to Computational Fluid Dynamics: the Finite Volume Method, Pearson education, 2007.
[24] B. Hadała, Z. Malinowski, M. Rywotycki, Energy losses from the furnace chamber walls during heating and heat treatment of heavy forgings, Energy 139 (2017) 298–314.
[25] Finkl Steel Inc., M., Saint-Joseph-de-Sorel, QC J3R 3M8, Canada., (n.d.).
[26] B. Ničeno, A.D.T. Dronkers, K. Hanjalić, Turbulent heat transfer from a multi-layered wall-mounted cube matrix: a large eddy simulation, Int. J. Heat Fluid Flow 23 (2002) 173–185.
[27] A. Hussain, Coherent structures-Reality and myth, (1983) [in turbulent shear flow].